

Studies on structural, electronic and optical properties of nonlinear optical material Li-In-Se and Li-In-Te under high pressure

Youchun Wang¹ and Hui Xie²

¹Linyi University

²Hebei Normal University for Nationalities

February 22, 2024

Abstract

The first-principle calculations is performed to search for the candidate stable structures for Li-In-Se and Li-In-Te system below 100 GPa for exploring nonlinear optical materials. A new structure with semiconductor properties has been successfully predicted, namely $R\text{-}3m$ LiInSe₂, may be a potential nonlinear optical material. At the same time, the electronic and optical properties confirm that the band gap of Pna_{21} LiInSe₂ is increasing under pressure, indicating that the optical damage threshold is increasing, which provides a new idea for improving the nonlinear optical properties of materials. In addition, the study of bonding properties shows that In atom exhibits negative valence state in the structure with high pressure or increased Li atom content, which is similar to Ga atom.

Studies on structural, electronic and optical properties of nonlinear optical material Li-In-Se and Li-In-Te under high pressure

Youchun Wang^{a*} Hui Xie^{b*}

^aCollege of Physics and Electrical Engineering, Linyi University, Linyi 267000, People's Republic of China

^bSchool of Physics and Electrical Engineering, Hebei Normal University for Nationalities 067000 , People's Republic of China

*Corresponding author: Email:

wangyouchun@lyu.edu.cn

huixie_hbun@163.com

Keyword: First-principles calculations; High pressure; Nonlinear optical material

Abstract

The first-principle calculations is performed to search for the candidate stable structures for Li-In-Se and Li-In-Te system below 100 GPa for exploring nonlinear optical materials. A new structure with semiconductor properties has been successfully predicted, namely $R\text{-}3m$ LiInSe₂, may be a potential nonlinear optical material. At the same time, the electronic and optical properties confirm that the band gap of Pna_{21} LiInSe₂ is increasing under pressure, indicating that the optical damage threshold is increasing, which provides a new idea for improving the nonlinear optical properties of materials. In addition, the study of bonding properties shows that In atom exhibits negative valence state in the structure with high pressure or increased Li atom content, which is similar to Ga atom.

Introduction

In recently, Lithium-containing ternary chalcopyrite compounds with various structural, electronic and optical properties have widely applied in the mid- and far-infrared regions, solar cells, light emitting diodes, nonlinear optical devices, optical frequency conversion [1-6]. The most important characteristic is that lithium based materials have a larger band gap and high birefringence properties, which make them more effective in nonlinear optical materials and femtosecond optical amplifier [7]. There are numerous theoretical and experimental studies on Li-base ternary chalcopyrite compounds, e.g. LiMX_2 ($\text{M}=\text{Al, Ga, In}$ and $\text{X}=\text{S, Se, Te}$) have received great attention.

Previous studies have indicated that the LiMX_2 ($\text{M}=\text{Al, Ga, In}$ and $\text{X}=\text{S, Se}$) belong to the orthorhombic structure, while tellurides are described by tetragonal structure [8-9]. Our studies on Li-Al-Te system and Li-Ga-Te system have confirmed that LiAlTe_2 [10] and LiGaTe_2 [11] are tetragonal structure at ambient condition. Many researchers have synthesized these compounds experimentally and studied their optical properties. Such as, Isaenko *et al.* [12] have synthesized the LiMX_2 crystal by using the Bridman-Stockbarger growth technique, and measured the band-gap values and transparency ranges. Grazhdannikov *et al.* [13] have obtained the LiGaTe_2 single crystal, and measured the X-ray diffraction and optical properties. Jia *et al.* [14] have grown the LiInSe_2 single crystal, and systematically studied the transmittance spectra, absorption coefficients and refractive indices. At the same time, researchers also have carried out many theoretical studies on the system. Ma *et al.* [15] have researched the lattice dynamics and thermodynamic properties of LiInX_2 ($\text{X}=\text{S, Se, Te}$) by the first-principles calculations. Lagoun *et al.* [16] have studied the elastic and piezoelectric properties of LiMX_2 ($\text{M}=\text{Ga, In; X}=\text{S, Se}$). Chandra *et al.* [17] have calculated the optical properties of LiInTe_2 at different pressures using first-principle method. The structural, electronic and optical properties of LiInSe_2 and LiInTe_2 have been researched by Ma *et al* with First-principle calculation method [18]. Using the first-principles calculations method Khanet *et al.* also have studied the anion-cation replacement effect on the structural and optoelectronic properties of the LiMX_2 ($\text{M}=\text{Al, Ga, In; X}=\text{S, Se, Te}$) compounds [19]. Recent research have demonstrated that LiInSe_2 has great potential as a solar cell [20]. Subsequently, Jia *et al.* [21] have found that LiInSe_2 was a promising high-performance anode material for lithium-ion batteries. In recent years, a series of theoretical studies on LiInSe_2 involving the structural, electronic, optical, dynamics, thermodynamic and optoelectronic properties [22-23]. In additional, researchers have used experimental means to study LiInSe_2 in the growth, thermal, optical and electrochemical properties [24-25]. As far as LiInTe_2 has been concerned, the elastic, piezoelectric, optical and electronic properties have been studied on experimentally and theoretically [26-27].

Computational methods

In this paper, in order to find all potential stable ground state structures of Li-In-Te system under extreme pressure, we have first performed variable-cell structural prediction simulations using the evolutionary algorithm [28-30] method based USPEX code. Then the extensive structure prediction have been executed using a swarm-intelligence based CALYPSO method and code, which enables global structure searching in conjunction with ab initio energetic calculations [31-32]. All structural optimizations are performed using the Vienna ab initio simulation package (VASP) [33-34] utilizing the projector augmented plane-wave (PAW) [35] method to describe the core-valence interaction. The plane-wave basis-set cutoff energy is set to 600 eV, and appropriate Monkhorst-Pack k-meshes [36] are employed with a resolution of $2\pi \times 0.03\text{\AA}^{-1}$ for Brillouin zone (BZ) sampling. Such conditions are adopted to ensure that all the enthalpy calculations are well converged to less than 1 meV per atom. In geometrical optimization, all forces on the atoms converge to less than 0.05 eV \AA^{-1} . Phonon calculations are performed based on the supercell approach [37] using the PHONOPY code [38].

Results and Discussions

In this paper, we performed variable-composition searches for stable Li-In-Se and Li-In-Te compounds at 1 atm, 30, 50 and 100 GPa using CALYPSO and USPEX codes. After a series of simulation calculations, the known structures $Pna\ 2_1$ LiInSe_2 and $I\ -42d$ LiInTe_2 have been discovered successfully, which are presented

in the ternary diagrams named in Fig. 1. The diagrams are determined by the thermodynamic convex cell which is a complete set of phases stable when their formation enthalpy (at T= 0 K) is negative. Meanwhile, we also uncovered several new structures at extreme pressures, namely, *R* -3*m* LiInSe₂, *I*_{mmm}Li₉InSe₂, *P* 4/*mmm*Li₆InSe, *I*_{mmm}Li₉In₂Se, *P* -3*m* 1 LiInTe₂, *I*_{mmm}Li₉InTe₂ and *P* 4/*mmm*Li₆InTe.

In order to determine the thermodynamic stability of the Li-In-Se and Li-In-Te system, the detailed enthalpy difference diagrams and formation enthalpy curves as a function of pressures after the phonon calculations are shown in Fig. 2. From Fig. 2 (a) we can learn that LiInSe₂ adopts the *Pna* 2₁ space group at ambient condition, changes to *R* -3*m* phase at 6 GPa. LiInTe₂ is stable with space group *I* -42*d* at ambient condition, then transforms into *P* -3*m* 1 phase at about 3.4 GPa, this process is consistent with that of LiAlTe₂ [39] and LiGaTe₂ [40] (Fig. 2 (b)). In our calculations, we find that the formation enthalpy of *I*_{mmm} Li₆InSe and Li₆InTe, *P* 4/*mmm*Li₉InSe₂, Li₉InTe₂ and *I*_{mmm}Li₉In₂Se are negative referring to Li₂Se and Li₂Te (Fig. S1 (a), (b), (c) (d) and (e)).

The new structures at different pressures we have found presented in Fig. 3. We can learn that in *R* -3*m* LiInSe₂, the Li atoms and Se atoms form an octahedron, as well as in *P* -3*m* 1 LiInTe₂, the Li atoms and Te atoms form an octahedron. In *P* 4/*mmm* Li₆InSe, each type of atom has a regular position, with the In atom occupying the vertex position, the Se atom occupying the central position, and the Li atom occupying the face and axis positions. For *P* 4/*mmm* Li₆InTe, the atoms occupy the same position as for *P* 4/*mmm*Li₆InSe, but the positions look different because of the way the primitive cells are selected. The atoms in *I*_{mmm}Li₉InSe₂ and Li₉InTe₂ occupy exactly the same position. However, the occupation of In and Se atoms in *I*_{mmm}Li₉In₂Se are in interchanged with those of the two kind of atoms in *I*_{mmm}Li₉InSe₂.

To further ascertain the dynamical stability of the new structures, we have calculated the phonon dispersion curves of Li-In-Se system and Li-In-Te system at 0 K using the PHONOPY code. The phonon spectrums of *R* -3*m* LiInSe₂, *P* -3*m* 1 LiInTe₂, *P* 4/*mmm* Li₆InSe and Li₆InTe, *I*_{mmm}Li₉InSe₂ and Li₉InTe₂, *I*_{mmm}Li₉In₂Se, at different pressures are chosen illustrated in Fig. 4. No imaginary phonon frequency exists in the whole Brillouin zone indicating that all the new structures are dynamically stable. However, several high-pressure structures become dynamically unstable after certain pressures. Therefore, in the pressure range we studied, the further phonon calculations combined with thermodynamic stability, we ensure that the approximate stable pressure ranges for *R* -3*m* LiInSe₂, *P* 4/*mmm* Li₆InSe, *I*_{mmm}Li₉InSe₂, *I*_{mmm}Li₉In₂Se, *P* -3*m* 1 LiInTe₂, *P* 4/*mmm* Li₆InTe, *I*_{mmm} Li₉InTe₂, are 6-30, 70-90, 40-90, 10-30, 3.4-100, 10-90 and 10-50 GPa, respectively.

The electronic properties research have been performed by the calculations of electronic band structures of Li-In-Se system and Li-In-Te system at different pressures. The selected electronic band structures are displayed in Fig. 5. From Fig. 5 (a) and (c) we can learn that *Pna* 2₁ LiInSe₂ and *I* -42*d* LiInTe₂ are direct band-gap semiconductors with 1.61 eV and 1.38 eV, which are consistent with previous studies [17-18]. We can see from Fig. 5(b), *R* -3*m* LiInSe₂ is an indirect band-gap semiconductor with 0.59 eV at 10 GPa, For other new structures (Fig. S2 (a-f)), all exhibit metallic characteristic. Interestingly, we find that the band-gap of *Pna* 2₁LiInSe₂ increase with increasing pressure. The increase of band gap indicates the increase of optical damage threshold. This provides a new idea for improving the nonlinear optical properties of materials. In order to find out the reason for the increase of band gap, the Partial Density of State (PDOS) for *Pna* 2₁LiInSe₂ were calculated (Fig. 6) and it was found that with the increase of pressure, the density of states became smooth and the hybridization increases. Therefore, we believed that band hybridization enhanced might be the reason for the increase of band gap.

The dielectric function is the link between the microphysical process of transition between bands and the electronic structure of crystal, which can reflect the band structure of solids and various kinds of light spectral information. The dielectric function can be expressed in the following formula: $\varepsilon(\omega) = \varepsilon_1(\omega) + i\varepsilon_2(\omega)$, where $\varepsilon_1(\omega)$ is the real part, $\varepsilon_2(\omega)$ is the imaginary part. The imaginary parts of dielectric function of *Pna* 2₁LiInSe₂ at 0 and 3 GPa and *I* -42*d*LiInTe₂ are plotted, which is presented in Fig. 7. The imaginary parts of dielectric function is related to the probability that the electrons absorbing photons, which represents the energy consumed to form the dipole. The absorption of photon by electron is the main characteristic of electron

band. From Fig.6 we can learn that the main peak position of *Pna* 2₁LiInSe₂ at 0 and 3 GPa is at 5.7 eV and 5.8 eV, the main attribution of the peak may be from the transition of electrons from Se p to In s orbitals. In *I* -42d LiInTe₂, the main peak is at 4.7 eV, the main attribution of the peak may be from the transition of electrons from Te p to In s orbitals. The difference of peak position indicates that the energy required for interband transition is different. The farther the peak position is, the more energy required for interband transition is, and the wider the band gap of the material is. The electronic band structure shows that the band gap of *Pna* 2₁ LiInSe₂ is larger than that of *I* -42d LiInTe₂, which is consistent with the location of the main peak.

Researchers have reported that the ABC₂ compounds with A-alkali metals, B-Ga, In, Tl and C-S, Se, Te are mixture of metallic-covalent-ionic bond properties. The A-C bonds are mainly ionic, whereas B-C bonds are preferentially covalent [40-41]. In our calculations of Li-In-Se system and Li-In-Te system, the electronic localization function (ELF) have been calculated, which are presented in Fig. 8. From Fig. 8 (a) and (b) we can learn that there are localized charge distribution between In and Se atoms for LiInSe₂ indicating the covalent bond properties. Meanwhile, less localized charge distribution is seen on the Li-Se bonds, showing the ionic bond between them. The results are similar to previous studies. However, for LiInTe₂ (Fig. 8 (c)), less localized electrons distribution between Li-Te bonds and In-Te bonds at ambient condition, indicating a significant degree of iconicity between Li cations, In cations and Te anions. For *P* -3m 1 LiInTe₂(Fig. 8 (d)), the results manifest the weak covalent In-Te bonds. The bonding properties of LiInTe₂ are same as the bonding properties for Li-Ga-Te system [42]. In addition, Figs. S3 also show that In and Te no longer form bonds, but Li and In form ionic bonds at high pressure in Li₆InSe, Li₉InSe₂, Li₉In₂Se, Li₆InTe and Li₉InTe₂.

To further understand the bonding properties, the atoms in molecules method (Bader charge analysis) [43] has been performed to analysis the charge transfer. The number of electrons gained and lost in Li-In-Se and Li-In-Te is list in Table 1. It can be found from Table 1 that for compounds LiInSe₂ and LiInTe₂, the number of electrons obtained by Se is more than that of Te, due to the difference in electronegativity. For LiInSe₂ and LiInTe₂, Li and In atoms approximately lose one electron to form [Li]⁺¹ and [In]⁺¹ ionic charge state, Te atoms and Se atoms gain one electron to form [Te]⁻¹ and [Se]⁺¹ ionic charge state. However, in Li₆InSe, Li₉InSe₂, Li₉In₂Se, Li₆InTe and Li₉InTe₂ the In atoms gain electrons, instead of losing electrons. Specific analysis found that all Se or Te atoms in Li₆InSe, Li₉InSe₂, Li₉In₂Se, Li₆InTe, and Li₉InTe₂ gain approximately two electrons to form [Te]⁻² ionic charge states. The In atoms gain about three electrons in this structures to form [In]⁻³ ionic charge states. In order to further verify the valence state of In ion, the charge distributions of these structures have been recalculated, the results are listed in Table 2. It is shown that the valence state of In atoms is about [In]⁻⁴ or [In]⁻⁵ ionic charge states. The result is slightly different from that of the Bader charge analysis, and requires a new step of verification. However, we can confirm that In atoms in these structures will have negative valence state when Li content increase and pressure increases.

Conclusions

In summary, the structural, electronic, optical and bonding characteristics of Li-In-Se and Li-In-Te system have been explored below 100 GPa by first-principle theory calculations. In our calculations, several new structures are found, namely, *R* -3mLiInSe₂, *Immm*Li₉InSe₂, *P* 4/mmmLi₆InSe, *Immm*Li₉In₂Se, *P* -3m 1 LiInTe₂, *Immm*Li₉InTe₂ and *P* 4/mmmLi₆InTe. The calculations of electron band structures for Li-In-Se and Li-In-Te system manifesting that *Pna* 2₁ LiInSe₂, *R* -3mLiInSe₂ and *I* -42d LiInTe₂ are semiconductor, other structures are metallic. Interestingly, the band gap of *Pna* 2₁ LiInSe₂ increases gradually under pressure, indicating an increase in the optical damage threshold, which provides new ideas for the subsequent improvement of the nonlinear optical properties. The imaginary part of dielectric function confirms the correspondence between optical spectrum and electronic energy band. Meanwhile, we have found that the In atoms present negative chemical valence state with Li content increasing or at high pressure.

Acknowledgements

This work was supported by the National Natural Science Foundation of China under Grants Nos. 12104127, Natural Science Foundation of Shandong Province (Nos. ZR2020QA060).

References

1. J. L. Shay, L. M. Schiavone, E Buehier, J. H. Wernick, *J. Appl. Phys.* **43** (1972) 2805–2810.
2. S. Wagner, J. L. Shay, B. Tell, H. M. Kasper, *Appl. Phys. Lett.* **1973**, 22, 351.
3. B. F. Levine, *Phys. Rev. B* **1973**, 7, 2600–2626.
4. S. Ozaki and S. Adachi, *J. Appl. Phys.* **2006**, 100, 113526.
5. I. G. Vasilyeva, R. E. Nikolaev, P. G. Krinitzin, and L. I. Isaenko, *J. Phys. Chem. C* **2017**, 121, 17429.
6. K. Wu, B. Zhang, Z. Yang, S. Pan, *J. Am. Chem. Soc.* **2017**, 139, 14885.
7. L. Isaenko, A. Yelisseyev, S. Lobanov, A. Titov, V. Petrov, J.-J. Zondy, P. Krinitzin, A. Merkulov, V. Vedenyapin, J. Smirnova, *Cryst. Res. Technol.* **2003**, 38, 379.
8. M. Bendjemai, H. Bouafia, B. Sahli, A. Dorbane, Ş. Uğur, G. Uğur, S. Mokrane, *Physica B: Condensed Matter.* **2020**, 599, 412463.
9. A. V. Kosobutsky, Yu. M. Basalaev, and A. S. Poplavnoi, *Phys. Status Solidi B* **2009**, 246, 364–371.
10. Y. C. Wang, F. B. Tian, D. Li, D. F. Duan, H. Xie, B. B. Liu, Q. Zhou, T. Cui, *Solid. State. Commun.* **2018**, 270, 58–64.
11. Y. X. Li, F. B. Tian, Q. Y. Zhou, M. X. Yang, Y. C. Wang, C. M. Shi, X. L. Wang, *Solid. State. Commun.* **2021**, 336, 114402.
12. L. Isaenko, I. Vasilyeva, A. Merkulov, A. Yelisseyev, S. Lobanov, *J. Cryst. Growth.* **2005**, 275, 217–223.
13. S. A. Grazhdannikov, G. K. Pavel, F. A. Kurus, L. I. Isaenko, A. P. Yelisseyev, M. S. Molokeev, *Mater. Sci. Semicon. Proc.* **2017**, 72, 52–59.
14. N. Jia, X. X. Xiong, S. P. Wang, T. T. Yu, B. Han, J. Qiao, C. N. Li and X. T. Tao, *Cryst. Eng. Comm.* **2018**, 20, 7802–7808.
15. T. H. Ma, L. Sun, C. Xu, Y. F. Chen, *J. Alloys. Compd.* **2011**, 509, 9733–9741.
16. B. Lagoun, T. Bentria, B. Bentria, *Comput. Mater. Sci.* **2013**, 68, 379–383.
17. S. Chandra and V. Kumar, *Lecture Notes in Electrical Engineering*, **2018**, 472, 165–170.
18. C.-G. Ma, M. G. Brik, *Solid. State. Commun.* **2014**, 203, 69–74.
19. A. Khan, M. Sajjad, G. Murtaza and A. Laref, *Zeitschrift für Naturforschung A* **2018**, 73, 0070.
20. M. Magesh, A. Arunkumar, P. Vijayakumar, G. AnandhaBabu, P. Ramasamy, *Opt. Laser. Technol.* **2014**, 56, 177.
21. N. Jia, M. Q. Zhang, B. Li, C. C. Li, Y. Y. Liu, Y. P. Zhang, T. T. Yu, Y. Liu, D. L. Cui, X. T. Tao, *Electrochim. Acta* **2019**, 320, 134562.
22. T. H. Ma, C. H. Yang, Y. Xie, L. Sun, W. Q. Lv, R. Wang, C. Q. Zhu, M. Wang, *Comput. Mater. Sci.* **2009**, 47, 99–105.
23. T. H. Ma, L. Sun, C. Xu, Y. F. Chen, *J. Alloys. Compd.* **2011**, 509, 9733–9741.
24. T. H. Ma, H. C. Zhang, J. J. Zhang, Z. T. Lei, C. Q. Zhu, C. H. Yang, *J. Cryst. Growth.* **2016**, 448, 122–127.
25. L. Dai, C. Tan, Z. H. Yan and Y. H. Xu, *Mod. Phys. Lett. B* **2016**, 30, 1650290.
26. A. H. Reshaka and M.G. Brikc, *J. Alloys. Compd.* **2016**, 675, 355–363.

27. V. Kumar and S. Chandra, *Cryst. Res. and Technol.* **2018**, *53*, 1800133.
28. A. R. Oganov, C. W. Glass, *J. Chem. Phys.* **2006**, *124*, 244704.
29. A. O. Lyakhov, A. R. Oganov, H. T. Stokes, Q. Zhu, *Comput. Phys. Commun.* **2013**, *184*, 1172-1182.
30. C. W. Glass, A. R. Oganov, N. Hansen, *Comput. Phys. Commun.* **2006**, *175*, 713-720.
31. Y. C. Wang, J. Lv, L. Zhu, Y. M. Ma, *Phys. Rev. B* **2010**, *82*, 094116.
32. Y. C. Wang, J. Lv, L. Zhu, Y. M. Ma, *Comput. Phys. Commun.* **2012**, *183*, 2063-2070.
33. G. Kresse, J. Furthmüller, *Phys. Rev. B* **1996**, *54*, 11169.
34. G. Kresse, J. Furthmüller, *Comput. Mater. Sci.* **1996**, *6*, 15-50.
35. G. Kresse and D. Joubert, *Phys. Rev. B* **1999**, *59*, 1758.
36. H J Monkhorst, J. D. Pack, *Phys. Rev. B* **1976**, *13*, 5188.
37. K. Parlinski, Z. Q. Li, Y. Kawazoe, *Phys. Rev. Lett.* **1997**, *78*, 4063.
38. A. Togo, F. Oba, I. Tanaka, *Phys. Rev. B* **2008**, *78*, 134106.
39. Y. C. Wang, F. B. Tian, D. Li, D. F. Duan, H. Xie, B. B. Liu, Q. Zhu, T. Cui, *Solid. State. Commun.* **2018**, *270*, 58-64.
40. Z. Z. Kish, E. Yu. Peresh, V. B. Lazarev, E. E. Semrad, *Inorg. Mater.* **1987**, *23*, 697
41. L. Isaenko, A. Yelisseyev, S. Lobanov, P. Krinitin, V. Petrov, J. J. Zondy, *J. Non-Cryst. Solids* **2006**, *352*, 2439-2443.
42. Y. X. Li, F. B. Tian, Q. Y. Zhou, M. X. Yang, Y. C. Wang, C. M. Shi, X. L. Wang, *Solid. State. Commun.* **2021**, *336*, 114402.
43. R. F. W. Bader, Atoms Molecules: A Quantum Theory (Clarendon: Oxford) **1990**.

Figure Captions:

Table 1. The Bader charge analysis for the Li-In-Se and Li-In-Te system.

Table 2. The Mulliken charge population analysis for $P\ 4/mmm$ Li_6InSe and Li_6InTe , $Immm\text{Li}_9\text{InSe}_2$ and Li_9InTe_2 , $Immm\text{Li}_9\text{In}_2\text{Se}$, respectively.

Fig. 1. The convex hull curves for Li-In-Se and Li-In-Te at 0 GPa.

Fig. 2. The enthalpy difference curves. (a) LiInSe_2 , (b) LiInTe_2 .

Fig. 3. Stable structure diagrams at different pressure. (a) $R\ -3m$ LiInSe_2 at 10 GPa, (b) $P\ 4/mmm$ Li_6InSe at 70 GPa, (c) $Immm\text{Li}_9\text{InSe}_2$ at 40 GPa, (d) $Immm\text{Li}_9\text{In}_2\text{Se}$ at 20 GPa, (e) $P\ -3m\ 1$ LiInTe_2 at 10 GPa, (f) $P\ 4/mmm$ Li_6InTe at 40 GPa, (g) $Immm\text{Li}_9\text{InTe}_2$ at 20 GPa, respectively.

Fig. 4. Phonon dispersion curves under different pressures. (a) $R\ -3m$ LiInSe_2 , (b) $P\ 4/mmm\text{Li}_6\text{InSe}$, (c) $Immm\text{Li}_9\text{InSe}_2$, (d) $Immm\text{Li}_9\text{In}_2\text{Se}$, (e) $P\ -3m\ 1$ LiInTe_2 , (f) $P\ 4/mmm\text{Li}_6\text{InTe}$, (g) $Immm\text{Li}_9\text{InTe}_2$, respectively.

Fig. 5. Electron band structure diagrams. (a) $Pna\ 2_1$ LiInSe_2 , (b) $R\ -3m$ LiInSe_2 , (c) $I\ -42d$ LiInTe_2 .

Fig. 6 The Partial Density of State (PDOS) for $Pna\ 2_1$ LiInSe_2 at 0 and 3 GPa.

Fig. 7. Imaginary part of dielectric function.

Fig. 8. Electron localization function (ELF) maps in the planes where the Li, In and Se or Te atoms lie for (a) $Pna\ 2_1\text{LiInSe}_2$ at 0 GPa, (b) $R\ -3m\ \text{LiInSe}_2$ at 10 GPa, (c) $I\ -42d\ \text{LiInTe}_2$ at 0 GPa, (d) $P\ -3m\ 1\ \text{LiInTe}_2$ at 10 GPa, respectively.

Table 1

<i>Pna2</i> ₁	Li	In	Se1	Se2				
charge	0.85	0.91	-0.89	-0.87				
<i>R-3m</i>	Li	In	Se1	Se2				
charge	0.84	1.02	-0.93	-0.93				
<i>P4/mmm</i>	Li1	Li2	Li3	Li4	Li5	Li6	In	Se1
charge	0.71	0.7	0.7	0.7	0.7	0.7	-2.4	-1.81
<i>Imm</i> _m	Li1	Li2	Li3	Li4	Li5	Li6	Li7	Li8
charge	0.74	0.74	0.74	0.74	0.72	0.72	0.75	0.75
	In	Se1	Se2					
	-2.9	-1.88	-1.87					
<i>Imm</i> _m	Li1	Li2	Li3	Li4	Li5	Li6	Li7	Li9
charge	0.75	0.75	0.75	0.75	0.75	0.77	0.77	0.757
	In1	In2	Se					
	-2.4	-2.5	-1.87					
<i>I-42d</i>	Li	In	Te1	Te2				
charge	0.84	0.7	-0.77	-0.77				
<i>P-3m</i> ₁	Li	In	Te1	Te2				
charge	0.85	0.62	-0.73	-0.74				
<i>P4/mmm</i>	Li1	Li2	Li3	Li4	Li5	Li6	In	Te1
charge	0.78	0.76	0.76	0.76	0.76	0.75	-2.75	-1.81
<i>Imm</i> _m	Li1	Li2	Li3	Li4	Li5	Li6	Li7	Li9
charge	0.75	0.75	0.75	0.75	0.72	0.76	0.76	0.73
	In1	Te1	Te2					
	-3.14	-1.78	-1.78					

Table 2

<i>P4/mmm</i>	Li1	Li2	Li3	Li4	Li5	Li6	In	Se1
charge	0.88	0.88	0.88	0.88	1.71	0.6	-3.98	-1.85
<i>P4/mmm</i>	Li1	Li2	Li3	Li4	Li5	Li6	In	Te1
charge	0.74	1.71	1.71	1.71	1.71	-1.35	-4.33	-1.88
<i>Imm</i> _m	Li1	Li2	Li3	Li4	Li5	Li6	Li7	Li9
charge	0.83	0.83	0.83	0.83	1.35	1.35	0.65	1.13
	In	Se1	Se2					
	-4.9	-2.01	-2.01					
<i>Imm</i> _m	Li1	Li2	Li3	Li4	Li5	Li6	Li7	Li9
charge	0.99	0.99	0.99	0.99	1.59	1.59	0.03	1.75
	In	Te1	Te2					
	-5.07	-1.8	-1.8					
<i>Imm</i> _m	Li1	Li2	Li3	Li4	Li5	Li6	Li7	Li9
charge	0.9	0.64	1.6	1.64	1.64	0.2	0.2	0.77
	In1	In2	Se					
	-3.83	-3.83	-1.74					

Fig. 1

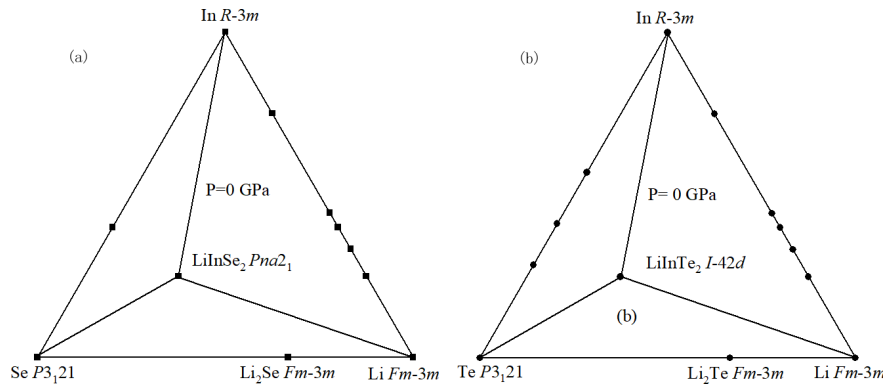


Fig. 2

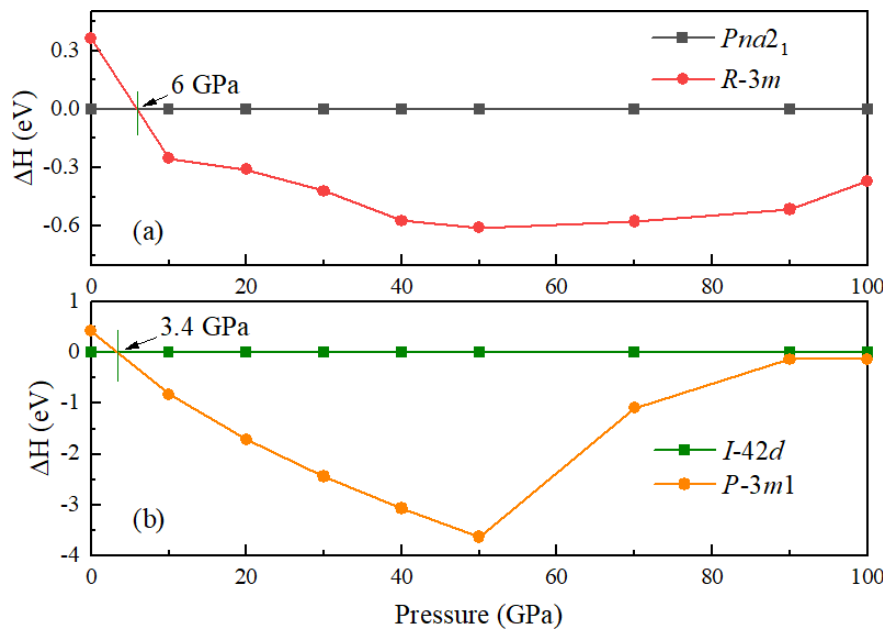


Fig. 3

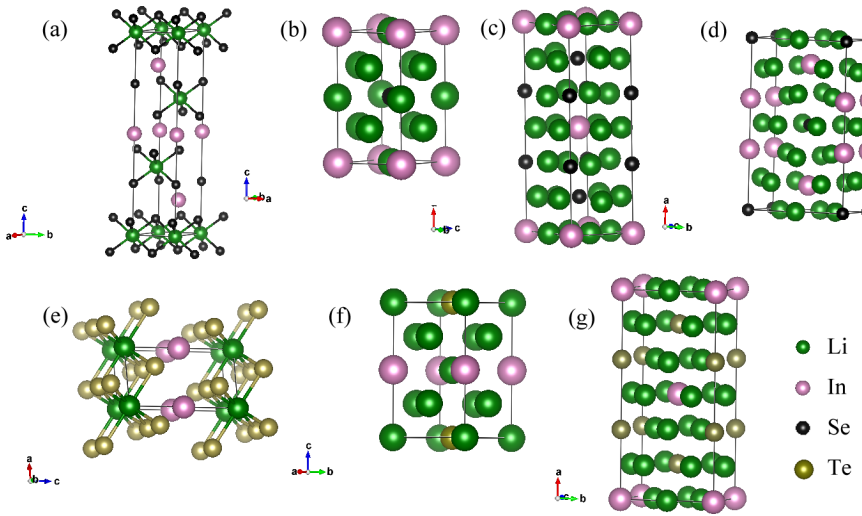


Fig. 4

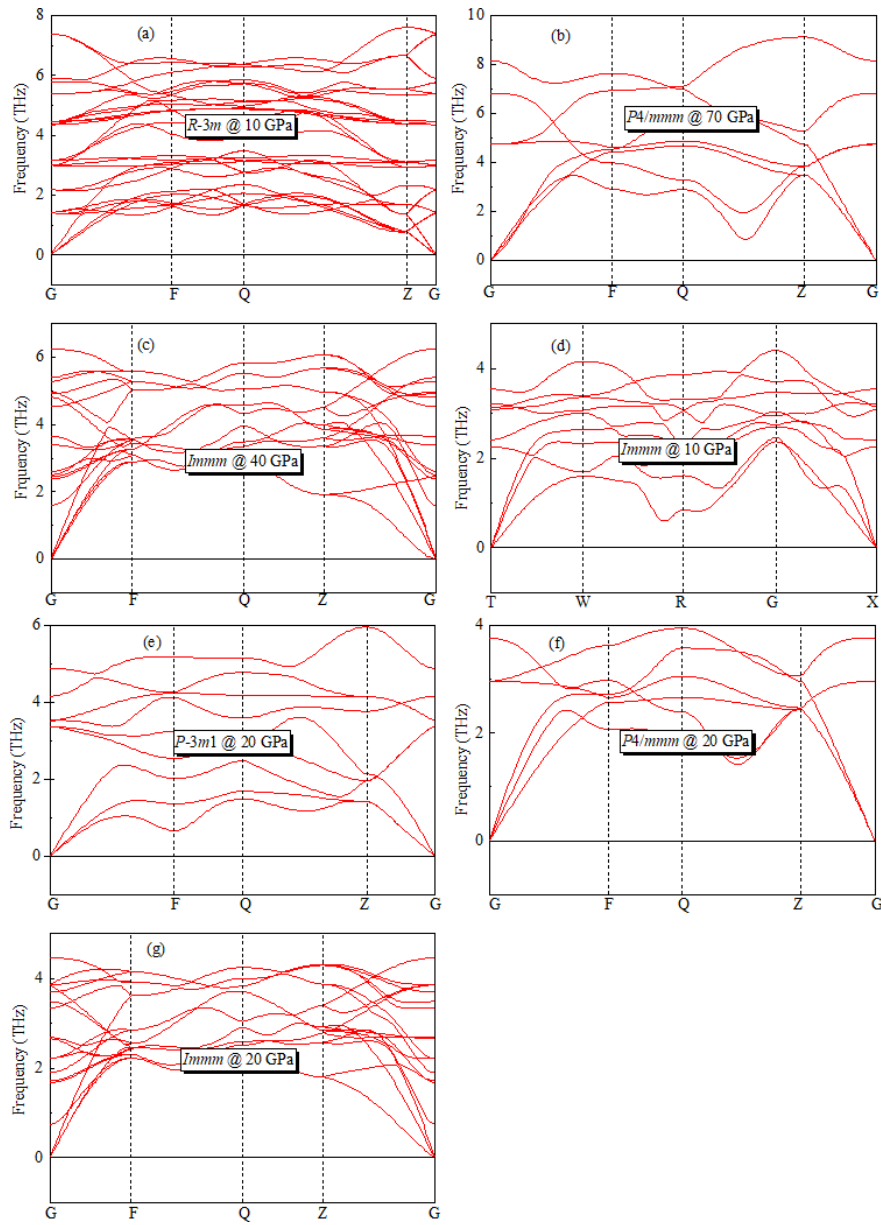


Fig. 5

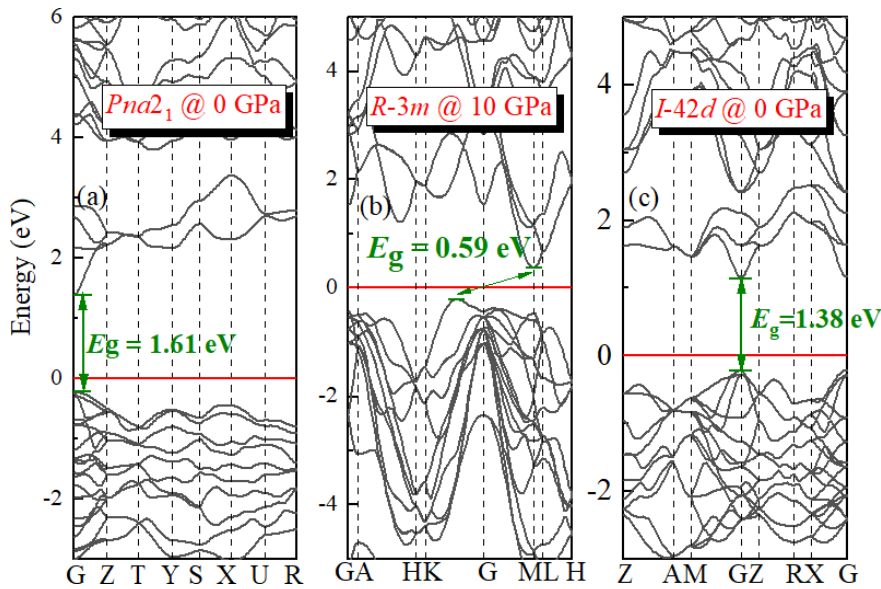


Fig. 6

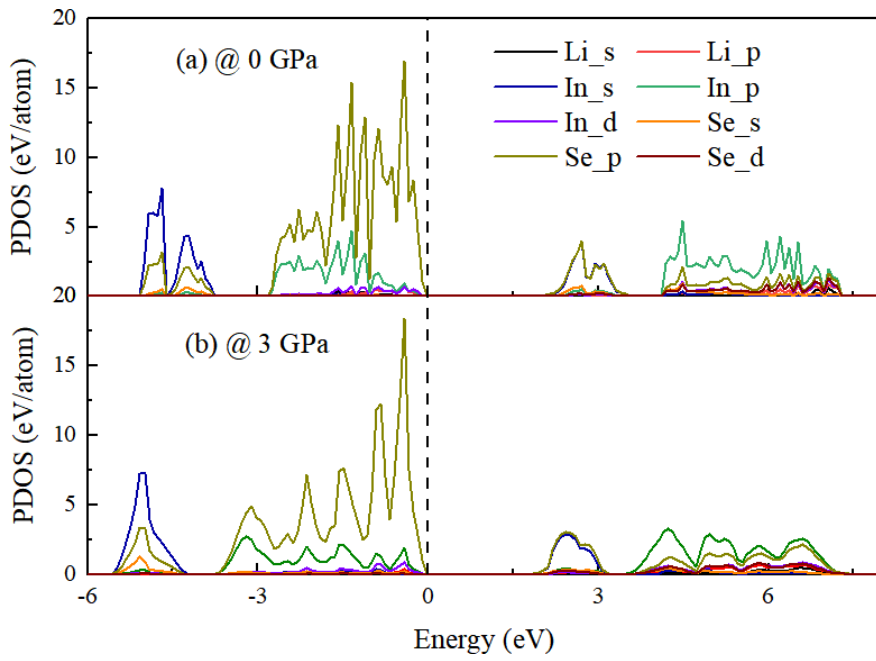


Fig. 7

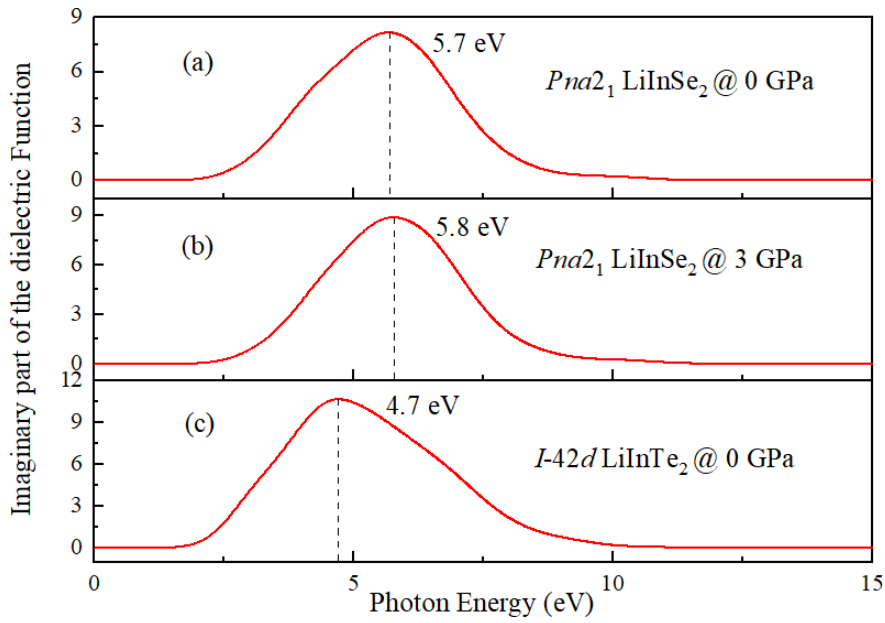


Fig. 8

